PAPER

Surface and bulk electronic structure of the unconventional superconductor Sr_2RuO_4: unusual splitting of the β band

To cite this article: V B Zabolotnyy *et al* 2012 *New J. Phys.* **14** 063039

New Journal of Physics
The open-access journal for physics

Surface and bulk electronic structure of the unconventional superconductor Sr_2RuO_4: unusual splitting of the β band

V B Zabolotnyy[1,7], E Carleschi[2], T K Kim[1,6], A A Kordyuk[1,3], J Trinckauf[1], J Geck[1], D Evtushinsky[1], B P Doyle[2], R Fittipaldi[4], M Cuoco[4], A Vecchione[4], B Büchner[1,5] and S V Borisenko[1]

[1] Institute for Solid State Research, IFW-Dresden, P O Box 270116, D-01171 Dresden, Germany

[2] Department of Physics, University of Johannesburg, P O Box 524, Auckland Park 2006, South Africa

[3] Institute of Metal Physics of National Academy of Sciences of Ukraine, 03142 Kyiv, Ukraine

[4] CNR-SPIN, and Dipartimento di Fisica 'E R Caianiello', Università di Salerno, I-84084 Fisciano (Salerno), Italy

[5] Institut für Festkörperphysik, Technische Universität Dresden, D-01062 Dresden, Germany

E-mail: v.zabolotnyy@ifw-dresden.de

New Journal of Physics **14** (2012) 063039 (13pp)
Received 20 February 2012
Published 28 June 2012
Online at http://www.njp.org/
doi:10.1088/1367-2630/14/6/063039

Abstract. We present an angle-resolved photoemission study of the surface and bulk electronic structure of the single layer ruthenate Sr_2RuO_4. As the early studies by photoemission and scanning tunneling microscopy were confronted with a problem of surface reconstruction, surface ageing was previously proposed as a possible remedy to access the bulk states. Here, we suggest an alternative way by demonstrating that, in the case of Sr_2RuO_4, circularly polarized light can be used to disentangle the signals from the bulk and surface layers, thus opening the possibility to investigate many-body interactions both in bulk and surface bands. The proposed procedure results in improved momentum resolution, which enabled us to detect an unexpected splitting of the surface β band. We discuss the origin of the splitting of the β band and the possible connection with the Rashba effect at the surface.

[6] Present address: Diamond Light Source Ltd, Didcot, Oxfordshire, OX11 0DE, UK

[7] Author to whom any correspondence should be addressed.

Contents

1. Introduction

Strontium ruthenates belong to the so-called Ruddlesden–Popper series of layered perovskites [1] and are well known for their unconventional p-type superconductivity [2, 3], metamagnetism [4], proximity to a quantum critical point [5, 6] along with the notable effects of spin–orbit coupling [7–11]. In particular, understanding the superconductivity in single-layered Sr_2RuO_4—the first unconventional copper-free oxide superconductor [2]—requires a detailed knowledge of its electronic structure. Active studies by means of photoemission [12–16], band structure calculations [7, 8, 17–19], Compton scattering [20] and de Haas–van Alphen (dHvA) measurements [21] reached a consensus as regards its low-energy electronic structure: the Fermi surface (FS) of Sr_2RuO_4 consists of three sheets, with the α and β sheets formed by quasi-one-dimensional (1D) out-of-plane Ru $4d_{yz}$ and $4d_{zx}$ orbitals, whereas the γ sheet is formed by the 2D in-plane Ru $4d_{xy}$ orbitals.

A characteristic feature of Sr_2RuO_4, which initially was quite perplexing to the photoemission community, is a $\sqrt{2} \times \sqrt{2}$ reconstruction due to slight rotations of the RuO_6 octahedra in the topmost layer [22]. The reconstruction implies doubling of the unit cell and thus folding of the surface Brillouin zone (BZ). As a result, a new set of surface-induced states with different underlying dispersions appears, so that both signals are seen superimposed in a typical angle-resolved photoemission (ARPES) experiment [23].

To overcome the problem of surface-related states it was suggested to cleave the sample at high temperature ($\sim$200 K), or age the sample surface. This recipe has been followed by the majority of the ARPES community [12–15, 24–26]. However, in the most recent scanning tunneling microscopy study [27] it was argued that high-temperature cleaving does not actually suppress the $\sqrt{2} \times \sqrt{2}$ surface reconstruction and that the major ageing effect is due to the increased surface disorder on the mesoscopic scale, which effectively blurs the superstructure replicas, so that they become less visible in ARPES FS intensity maps. Obviously such surface disorder equally scatters photoelectrons not only from the replicas, but also from the original bulk bands, resulting in a disorder-induced broadening of photoemission peaks [28–30]. To account for these adverse effects, we have performed measurements at extremely low temperatures ($T < 2$ K), analyzing spectra measured from both 'aged' and 'fresh' samples. We find that alongside the earlier proposed remedy of high-temperature cleaving, one may rely on the use of circularly polarized light to establish the origin of bulk and surface features. Owing to the minimized surface degradation we now observe bulk α, β, γ bands and their surface counterparts *along with an additional new feature*. According to its dichroic pattern, the new feature must be yet another surface counterpart of the β band. Since there are numerous

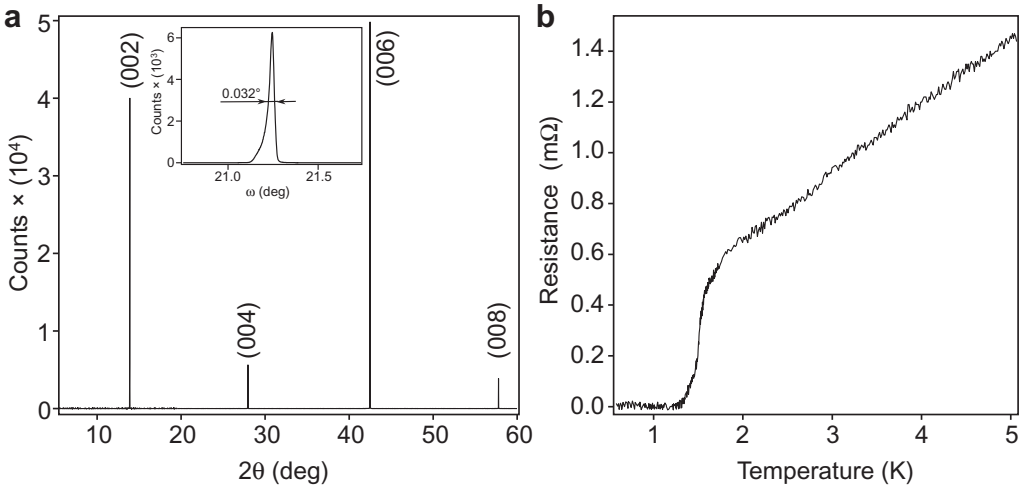

Figure 1. (a) θ–2θ XRD pattern on the (001) surface of Sr_2RuO_4. The inset contains the 2θ–ω rocking curve scan. (b) Resistance of Sr_2RuO_4 samples as a function of temperature.

examples where the surface state undergoes splitting due to the spin–orbit interaction we suggest that fully relativistic calculations might be needed to understand the origin of the new surface state.

2. Methods

The composition of the samples used in this study has been characterized by x-ray diffraction (XRD) and electron backscatter diffraction. The structure and crystalline qualities were assessed by a high-resolution x-ray diffractometer (Philips, model X'Pert MRD), with Cu K-α source. The typical XRD pattern taken on a cleaved surface of the Sr_2RuO_4 crystals is shown in figure 1(a). All the diffraction peaks can be identified with the expected (001) Bragg reflections of the Sr_2RuO_4 phase, confirming the absence of any spurious phase. The high quality of the crystals is also confirmed by the narrow peak width in the rocking curve shown in the inset to figure 1(a) (full width at half maximum, FWHM $= 0.032^\circ$). The purity of the crystals is supported by ac susceptibility and resistivity measurements (figure 1(b)), where the narrow superconducting transition with $T_c = 1.34$ K, is a signature of a low impurity concentration [31].

All photoemission measurements were performed at the BESSY 1^3 ARPES station equipped with a SCIENTA R4000 analyzer and a Janis ^{3}He cryostat. Spectra presented in this paper were recorded from high-quality Sr_2RuO_4 samples cleaved at high/low temperature. The high-temperature cleave was performed on the transfer arm at $T = 300$ K, just before transferring the sample to the cold finger of the cryostat. For the low-temperature cleave the samples were first mounted on the cold finger of the cryostat and after pre-cooling down to $T \sim 15$–40 K the cleave was performed. Sample orientation and determination of high symmetry directions were done using wide overview FS maps, one of which is shown in figure 2.

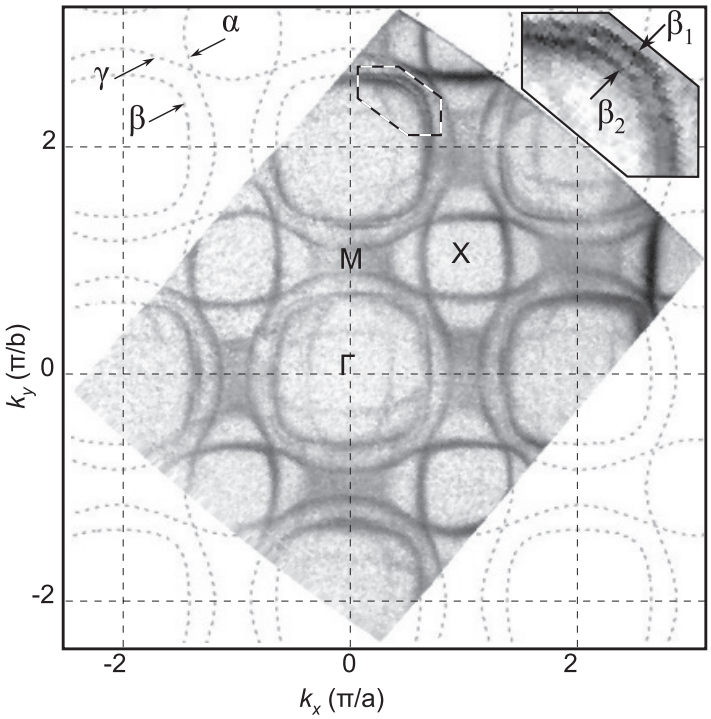

Figure 2. Typical overview FS map used for sample orientation. α, β and γ denote three bands contributing to the FS of Sr_2RuO_4. The underlying set of contours extend the experimentally observed bands over the whole extended BZ picture. The inset shows the splitting of the β band. The corresponding domain is marked on the FS by the dotted line. The map was measured using horizontally polarized light with $h\nu = 100\,\mathrm{eV}$.

3. Results and discussion

In figure 2, we present the experimental FS map given by the distribution of the photoemission intensity at the Fermi level (FL) recorded over a voluminous part of the reciprocal space in the superconducting state of Sr_2RuO_4. The dark features correspond to regions where the bands cross the FL. In agreement with the earlier measurements, one can identify the square-like contour centered at the X point as corresponding to the α band. The other two, more rounded features centered at the Γ point, must be formed by the β and γ bands. The surface reconstruction results in the appearance of replica bands, shifted by the vector $\overline{\Gamma X}$.

A closer look reveals that the picture is more complex. The first and the most obvious detail can already be seen in the FS map (figure 2). The FS contour corresponding to the β band appears to be split (see the inset), with the splitting most notable along the diagonal of the BZ. The value of the momentum splitting between the two features can be followed in figure 3.

In figure 4(a), we show the FS measured with lower excitation energy, to get better effective energy and momentum resolution, using a sample cleaved at low temperature $T = 16\,\mathrm{K}$. The FS map is supplemented with an energy–momentum cut, which allows one to trace the energy dispersion of the spectral features. To classify all the observed bands, we label the trivial α band replicas arising due to the surface reconstruction as α^{r}, the two features apparently related

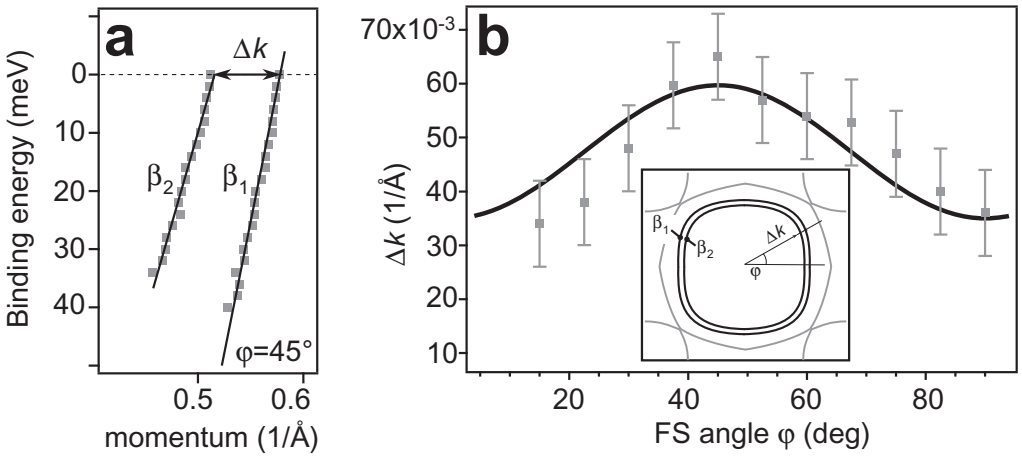

Figure 3. Momentum splitting between the β_1 and β_2 bands along the FS contour. (a) Extracted momentum distribution curve (MDC) dispersion for the energy–momentum cut at $\varphi = 45^\circ$ and momentum splitting at the FL. The square symbols are the MDC peak positions for the two features. (b) Momentum splitting at the FL, Δk, over the Fermi contour. The black line is the fit to the function $A\cos(\varphi) + B$.

to the β band are denoted as β_1 and β_2, while the features related to α and γ are labeled accordingly. Considering the energy–momentum cut it is also easy to see that the α and γ features, which appear as individual bands in the FS map, actually consist of pairs of bands with slightly different Fermi velocities.

Obviously, the multitude of the features we observe in the spectra must result from a superposition of bulk and surface states. An effective method to discern between them is based on accounting for the surface-induced electromagnetic fields [32–36] and consequently different modification of the photoemission matrix element for the states primarily localized at the surface and in the bulk. A strict calculation of such fields requires taking into account the nonlocal dielectric function $\varepsilon(\mathbf{r}, \mathbf{r}', \omega)$ [37–40]. For excitation energies below the plasma frequency the amplitude of the generated field may significantly exceed the intensity of the incident light, and thus substantially enhance the photo-yield [41]. At higher excitation energy this enhancement is weak, but there is a finer effect. To understand the idea behind this, let us consider the simplest estimate for the photoemission intensity in the form of Fermi's golden rule

$$w_{\mathrm{i}\to\mathrm{f}} \sim \frac{2\pi}{\hbar}\left|\langle \mathrm{f}|\hat{H}_{\mathrm{pert}}|\mathrm{i}\rangle\right|^2 \delta(E_\mathrm{f} - E_\mathrm{i} - \hbar\omega), \tag{1}$$

where $\hat{H}_{\mathrm{pert}} = -\frac{ei\hbar}{mc}(\mathbf{A}\nabla + \frac{1}{2}\mathrm{div}\,\mathbf{A})$ is the perturbation due to the electromagnetic field. The spatially oscillating field results in a nonzero div $\mathbf{A}$ term in that region, consequently modifying the matrix element for the surface localized states [42]. The depth down to which the term div $\mathbf{A}$ affects the matrix elements depends on the particular field pattern near the surface [33, 43, 44]. A basic insight can be obtained considering a relatively simple jellium model. Employed to describe a free-electron metal [45, 46], the model shows that the vector potential of the electromagnetic wave $\mathbf{A}(\mathbf{r})$ undergoes quickly decaying Friedel-like oscillations with a characteristic scale of a few angstroms. In a more recent study of TiS_2, which is closer to the case of layered Sr_2RuO_4, the crystalline structure was taken into account [47]. This study

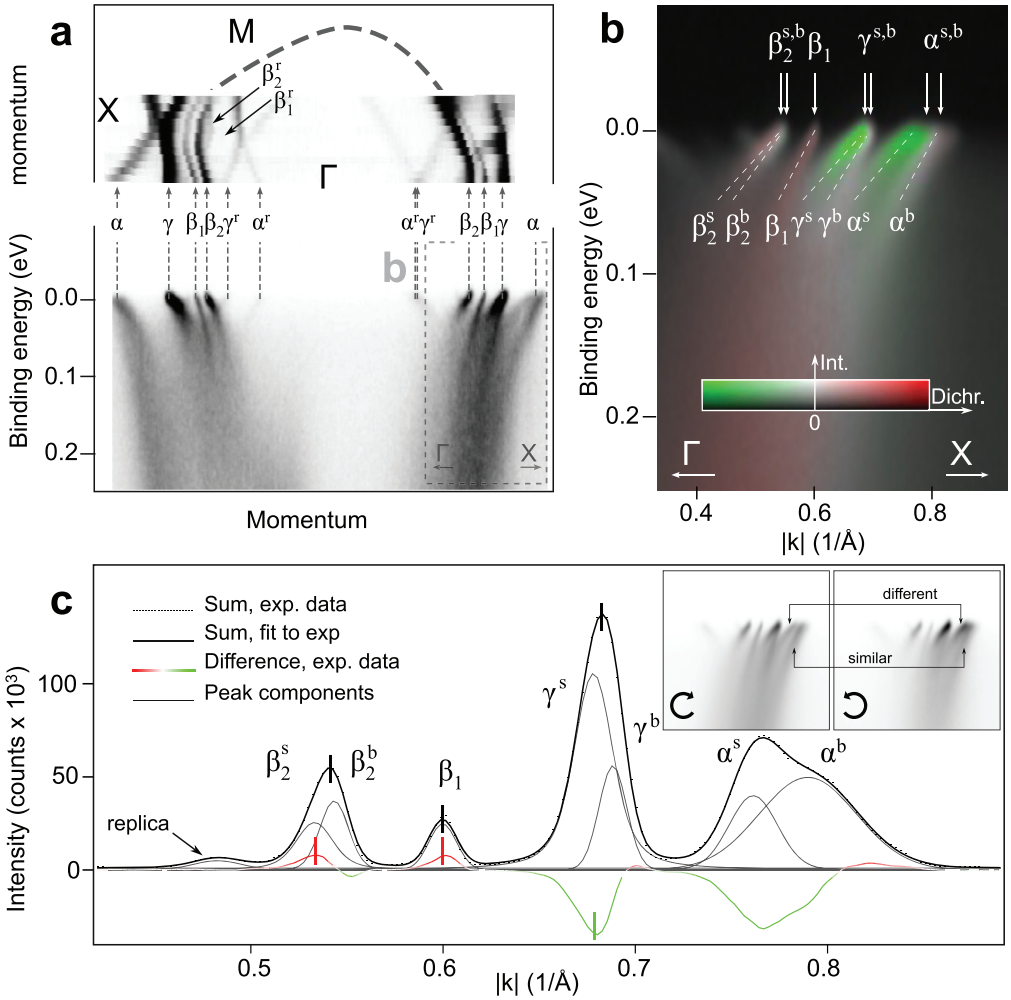

Figure 4. (a) FS map and energy–momentum image, used to index features seen in spectra, $h\nu = 50\,\mathrm{eV}$, circularly polarized light of positive helicity, $T = 1.3\,\mathrm{K}$. The faded letter b and the dashed rectangular denote part of the image shown in the next panel. (b) Circular dichroism. The intensity in the false color image represents the sum of the signals obtained with circular right (CR) and circular left (CL) polarized light, while the color corresponds to the dichroic signal CR − CL. Panel (c) contains the sum and difference energy distribution curves (EDCs) taken at 2 meV binding energy. The sum signal is fitted with a set of Voigt profiles; separate components are shown in thin black line, the fit to the total signal in thick black line. The inset to the panel (c) demonstrates that the dichroic effect can already be seen in a pair of spectra measured with opposite helicities.

demonstrates that the rapid changes in $\mathbf{A}(\mathbf{r})$ occur within a thin surface layer with characteristic thickness of about one unit cell along the normal to the surface.

To realize the consequences of such an oscillating field, one can consider the simplest model that accounts for the div $\mathbf{A}$ term at the surface region [48]. In particular, approximating the final state by a plane wave $|\mathrm{f}\rangle = |\mathrm{e}^{\mathrm{i}\mathbf{kr}}\rangle$ and taking for the incident light a circularly polarized

plane wave $\mathbf{A}(\mathbf{r}) = \mathbf{A}_C \cos(\omega t - \mathbf{qr}) + \mathbf{A}_S \sin(\omega t - \mathbf{qr})$ it is easy to obtain for the circular dichroism

$$D \equiv dw_{i,f}^{cr} - dw_{i,f}^{cl} \sim |\langle i|\, e^{i\mathbf{kr}}\rangle|^2 \left\{ \left| \mathbf{A}_C i\mathbf{k} + \mathbf{A}_S \mathbf{k} + \frac{1}{2}\mathrm{div}\, \mathbf{A}_\perp \right|^2 - \left| \mathbf{A}_C i\mathbf{k} - \mathbf{A}_S \mathbf{k} + \frac{1}{2}\mathrm{div}\, \mathbf{A}_\perp \right|^2 \right\}. \quad (2)$$

Since $|\mathbf{A}_C i\mathbf{k} - \mathbf{A}_S \mathbf{k}| = |\mathbf{A}_C i\mathbf{k} + \mathbf{A}_S \mathbf{k}|$, in contrast to the surface bands, the dichroism within this model should vanish for the bulk states for which $\mathrm{div}\, \mathbf{A} \approx 0$ [49]. It is important to mention that the assumption of a plane wave is relatively good for high excitation energies, while at low excitation energies there must be deviations resulting in additional dichroism for bulk states as well.

Before exploiting the dichroism in practice, another brief clarification appears to be necessary. It has already been some time since the alleged circulating current (CC) phase, predicted to exist in the pseudogap state of cuprates by Chandra Varma [50], entered the focus of the ARPES community [51, 52]. The mysterious phase was expected to result in a detectable circular dichroism in photoemission spectra. One of the difficulties in detecting this phase was caused by the weakness of the CC-dichroism. Consequently, all other sources of dichroism had to be eliminated—including the routinely observed surface-related one that we are going to use in the current work. The elimination could only be achieved in the high symmetry directions, which imposed unprecedented requirements on sample alignment. As was shown by Borisenko *et al* [52], the CC-dichroism in cuprates is as high as 0.06% (if any). At the same time a small deviation from a high symmetry direction brings into play the 'geometric' dichroism, which may be as high as ~40%. The sole reason for this historical digression is to bring to the reader's attention that currently we are not dealing with the CC-dichroism (or a similar one) and the above-mentioned difficulties are not relevant to the current study.

Thus here we can utilize this qualitative distinction to separate the surface and bulk bands in Sr_2RuO_4. The results are shown in figure 4(b). In order to facilitate the comparison between the bands exhibiting circular dichroism and those with negligible dichroism, we plot them in one image, where the brightness corresponds to the sum of intensities obtained with opposite polarizations (CR + CL) and the color, ranging from green through white to red, encodes the dichroism strength (CR − CL). As can be seen from the map shown in figure 4(a), the energy–momentum cut we have selected is optimal for highlighting all features. The rightmost pair of dispersing features (α^s, α^b in figure 4(b)) forms the α pocket of the FS. Now, with the dichroic pattern we can see that the two bands are qualitatively different. The steeper band (α^b) exhibits virtually no dichroism, based on which we conclude that this must be a bulk band. The slowly dispersing band (α^s) is strongly dichroic, therefore we believe this one has to be a surface related counterpart of the α band. This identification is in agreement with earlier experimental work where the double structure of the α band was resolved [23] as well as with the theoretical calculation from [12].

Exactly the same dichroic pattern is also observed for the γ feature, except for the fact that the splitting at the FL is negligibly small, so that owing to the difference in the Fermi velocities the two counterparts can only be seen clearly separated at binding energies close to 50 meV. Here again the surface component (γ^s) has a higher renormalization compared to that of the bulk (γ^b). According to the dichroic image, the feature corresponding to the β_2 band consists of two components as well, but unlike the α band the splitting between them is quite small, approaching approximately 0.015 $Å^{-1}$ at the FL. In the dichroic pattern (figure 4(b)) this is manifested as a red shade on the left side, and a white shade on the right side of the composite surface + bulk β_2 feature.

While the complex color plot shown in figure 4(b) is convenient to demonstrate the distribution of the dichroism in energy–momentum space, it is not that usable when a judgement on the absolute values is needed. The absolute value is demonstrated in figure 4(c). The strength of the dichroism can already be judged by comparing a pair of spectra measured with opposite light helicities that are shown as the inset to figure 4(c). In order not to rely solely on the color scale images, but at the same time avoid cluttering the graph with a messy 'waterfall', in figure 4(c) we plot the sum and difference of *single* MDCs taken at 2 meV binding energy with opposite circular polarizations. The chosen binding energy guarantees that no replica band overlaps with the features of interest; two such replicas can be seen in figure 4(b), and one of those in the narrower momentum window of figure 4(c). As one can clearly see, the difference signal is not weak at all, and for some peaks amounts to about 20–30% of the sum intensity, so the observation can hardly be attributed to some kind of imbalance or misalignment. Another remarkable observation is that for the composite features (like $\beta_2^{s,b}$ or $\gamma^{s,b}$, but not for the single β_1) the centroids of the difference (marked by the vertical colored bars) coincide with the position of the surface components, which is a natural consequence of strong dichroism in one component and weak dichroism in the other one. The effect is most prominent for the pair of $\alpha^{s,b}$ features with the largest momentum separation, but also remains clearly detectable for the closest $\beta_2^{s,b}$ pair.

From the peak decomposition presented in figure 4(c), it becomes clear that the splitting of the β_2 feature can be *independently* inferred from the line shape analysis, without relying on the dichroism data. For instance, if one compares the width of the β_2 feature to the width of the single β_1, the former appears notably broader (see FS map in figure 4(a). One may presume that the broader appearance of the feature is caused by, say, a different impurity scattering. However, this assumption would be inconsistent with experimental observation, since increased scattering results in a symmetric peak broadening, while the β_2 feature has a clear shoulder. This argument can receive a stricter development in the form of line shape analysis. In figure 5, we show an MDC containing contributions from β_1, β_2 and γ features. To completely equalize the detector sensitivity along the angular direction, we have normalized the spectrum to the nonzero spectral weight present above the FL (background). This spectral weight is due to the higher harmonics in the spectrum of synchrotron light, which excite states with high binding energy that have no angular dependence.

Assuming that both β_2 and γ features are split into surface and bulk counterparts, the MDC shown in figure 5 can be nicely fitted by five Voigt profiles [53]. At the same time the three-peak model, i.e. the one assuming no splitting of the β_2 and γ features, results in obvious misfits for both β_2 and γ features. There are notable and characteristic misfits at the wings as well as at the maxima. The shading in the lower panel of 5(b) shows the pattern of residuals $(+ - + -)$ for the β and γ peaks, proving that the three-peak fit is statistically infeasible. This once again suggests splitting of the γ and β_2 bands, in agreement with the conclusion drawn from the dichroic data.

Therefore we see that the composite surface + bulk structure also holds for the γ- and β_2-pairs with progressively smaller splitting. In particular, this gradual decrease in momentum splitting can be seen in the notably broader FS contour for the composite α pocket as compared to the other bands (see figure 2 and figure 4(a).). All three surface components are also seen replicated in the new BZ. When going from the Γ- to the X-point in figure 4(a), first the α and γ replicas are seen to cross, then comes the β_2^{Γ}-replica which forms a tiny lens when considered together with the barely split β_2-pair. This is in agreement with earlier ARPES studies [12, 13, 15]. In this light the feature that we labeled as β_1 appear to be special as it does not fit

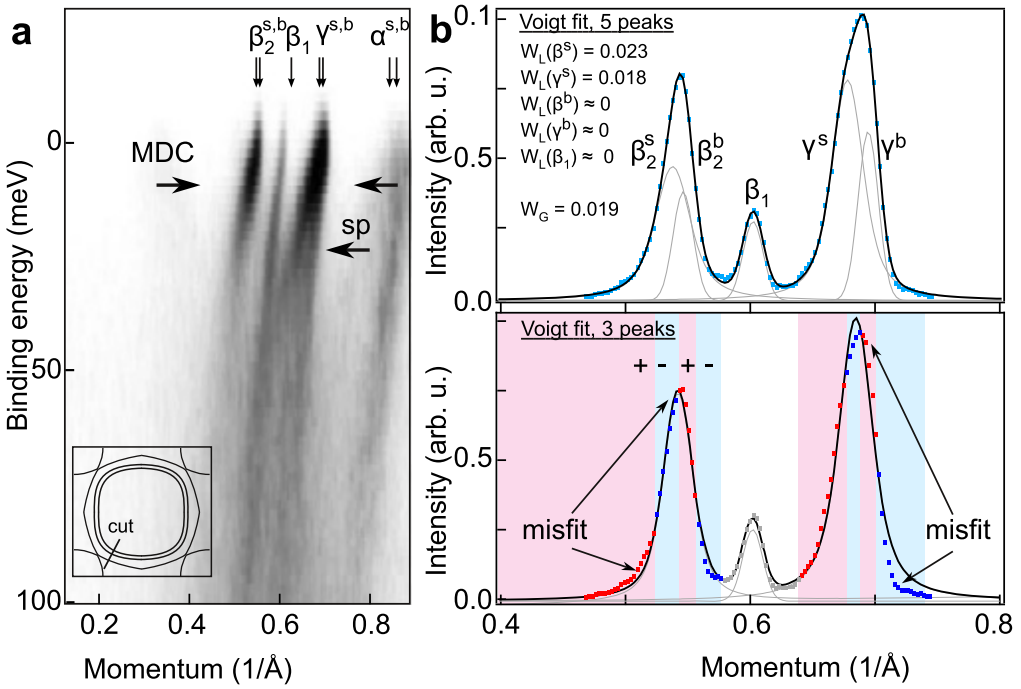

Figure 5. (a) Energy–momentum cut through the β_1, $\beta_2^{s,b}$ and $\gamma^{s,b}$ bands. The arrow marked with 'sp' denotes the energy at which splitting of the γ feature can be seen. The other two arrows denote the energy position and momentum range for the MDC shown in (b). The symbols represent the experimental data, while the fit with the five and three Voigt profiles is shown by the line. The Gaussian FWHM for the five-peak fit was held constant at the value corresponding to the experimental angular resolution, while all other parameters were left free. The spectrum was measured with 50 eV excitation energy, using circularly polarized light, which helps to enhance the β_2^b feature.

into the simple picture of three main bands and their replicas, whereas the strong dichroism (red color) points to its surface origin.

Based on our ARPES data we conclude that the new β_1 feature *must* be of surface origin, and additionally taking into account the form of the supported FS, we find that it has to be yet another surface counterpart of the bulk β band. Also, the narrower momentum width suggests a higher quasiparticle life-time and negligible k_z dispersion, which both would be distinct properties specific to a true surface state. Obviously this is not the whole story, and it is interesting to find out why such a surface feature exists. Appearance of the two surface counterparts of the β band would imply that the β band undergoes unexpected splitting. There are two likely reasons for this: a Zeeman splitting due to a source of time reversal symmetry breaking at the surface, or it may be due to a Rashba coupling originated by the surface confinement potential. The first case would imply the occurrence of a spontaneous magnetic moment at the surface, most probably driven by the atomic Coulomb interaction as for a Stoner ferromagnet, with a distinct orbital character, since a significant splitting is observed only for the β band. Although the scenario of a ferromagnetic instability at the surface has been considered in [22] to be stabilized by rotations of the octahedra, the proposed mechanism refers to the d_{xy}

band and not to the d_{yz} ones. Besides, so far there has been no experimental evidence of surface ferromagnetism in the Sr_2RuO_4 compound.

Concerning the possible role of the Rashba coupling, it is well known that the surface breaks spatial inversion symmetry, so there is an effective potential with a finite gradient along the surface normal and thus an electric field in this direction which manifests itself in the work function. If one considers the expression for the Rashba coupling within the nearly free-electron approximation and replaces the momentum operator with the k-vector, then for a typical amplitude of the effective potential at the surface one would get a splitting of the order of 10^{-6} eV. Nevertheless, it has been shown both in a simplified tight-binding picture [54] and within first-principles approaches that the strength of the Rashba coupling can be connected to the product of the amplitude of the intra-atomic spin–orbit coupling and to a parameter that describes the asymmetry of the wave function close to the surface [54] as well as to the admixture of d- and p-orbitals at the surface that is relevant to provide a significant expectation value of the weighted potential gradient [55]. Such know-how has been successfully applied to explain the differences in the splitting for Au(111), Ag(111), Lu(0001) as well as for the Li/W(110) and Li/Mo(110) systems [56–58]. Applying these considerations to the case of the Sr_2RuO_4 system, one would see that both the strength of the intra-atomic spin–orbit (estimated to be about 160 meV owing to the large Z of the Ru atom [7, 59, 60]) as well as the greater d–p hybridization due to the extended Ru-4d bands point to a significant enhancement of the Rashba coupling.

Considering the orbital character of the observed splitting, it is worth noting that due to the strong 2D character of the d_{xy} band the effect of the asymmetric surface potential for a [001] surface is weak for this orbital and in turn would not yield a significant Rashba splitting. On the other hand, since the α and β bands have the same orbital character it is natural to expect a similar Rashba parameter for the two pockets formed by the corresponding surface bands. In the case of parabolic bands the energy splitting at the FL is proportional to the size of the pocket: $E_{\pm} = \hbar^2 k_F^2/2m^* \pm \alpha_R k_F$ [57, 61]. Since the α pocket is about twice as small as the β one, this would roughly suggest a twice smaller Rashba splitting for the α pocket, so that the splitting of this surface contour is likely to remain unresolved and/or hidden by the bulk band. Accounting for the intra-atomic spin–orbit within a tight-binding description one can obtain a difference factor of about 3–4 in the splitting of the α and β bands, depending on the choice of the microscopic parameters.

Finally, although the Rashba coupling appears to be a possible cause for the observed splitting in the surface β band and a much smaller—thus undetected—splitting in the α band, we would like to point out that a full microscopic analysis, based on first-principles fully relativistic approaches, which include both the surface effects as well as the intra-atomic spin–orbit coupling, is required to quantitatively address the effect of the Rashba interaction.

Since the experimental FS of Sr_2RuO_4 is measured in more detail now, it is interesting to see how our observation compares to the model FS reconstructed from the dHvA data [21]. In figure 6, we show an ARPES FS acquired from the sample cleaved at 300 K with the dHvA contours overlapped over them. From inspection of figure 6 we note that the differences between the dHvA model and the ARPES FS contour for the bulk bands occur mainly for the α and the β bands, being largest for the k_F crossings *along the diagonals* of the BZ. For example, according to the dHvA *fits* the α pockets are expected to be rounder than those directly measured with ARPES. A space for possible refinements in the form of the pockets, especially the α one, is apparent not only from the current work but also from numerous earlier works [12, 14, 24], and

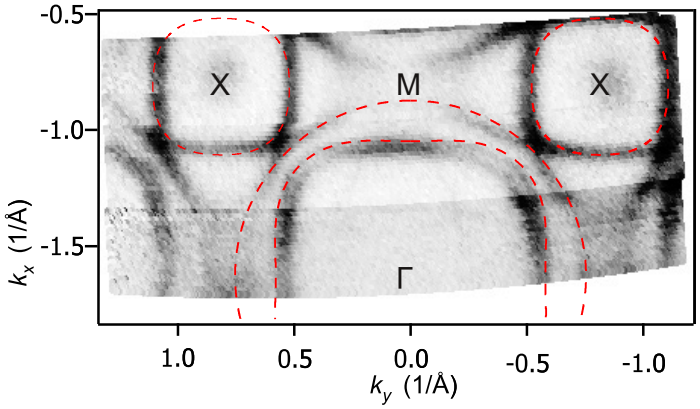

Figure 6. FS map measured at 40 K from the 'aged' sample cleaved at 300 K. Note the vanishing of the α band replicas. The overlapped contours are the results of dHvA fits [21].

is most notable in the data by Shen *et al* [15]. Since for both β and α pockets the dHvA model used in [21] includes only the lower harmonic for the in-plane warping data ($k_\phi \sim \cos(4\phi)$), actually extracted from early ARPES data, and neglects the higher-order harmonics, which are responsible for the detailed form of the FS, we believe that details of the FS, in particular positions of the k_F crossings at the BZ diagonal, are not precisely captured by the model. Necessary modifications of the model are likely to be achieved by the inclusion of higher-order harmonics, $k_\phi \sim \cos(4n\phi)$, $n \geqslant 2$. These extra terms would affect the Fermi contour only in small portions of the BZ, thus the overall agreement with the dHvA frequencies for Sr_2RuO_4, as contrasted with other compounds [62, 63], would remain unchanged.

4. Summary and conclusions

Despite common opinion on the extreme surface sensitivity of angle-resolved photoemission spectroscopy [64–66], and the detrimental effects of surface states introduced upon sample cleavage, we have demonstrated that the method can be successfully tuned to study bulk as well as surface states. In a certain sense, the suggested strategy outbalances the commonly used surface degradation approach, preserving the high-energy and -momentum resolution of the method. This allowed us to detect a new feature in the electronic structure of Sr_2RuO_4: the unexpected surface band, which is likely to be related to the strong spin–orbit coupling effects in this compound. We also note that the dHvA parameterization of the Sr_2RuO_4 can still be improved by inclusion of higher cylindrical harmonics, to better reproduce the form of the α pocket [21].

Acknowledgments

We acknowledge useful discussions with Professor Jeroen van den Brink, Dr Klaus Koepernik and Dr Felix Baumberger. The project was supported by DFG grant ZA 654/1-1. EC and BPD thank the Faculty of Science at the University of Johannesburg for travel funding. MC, RF

and AV acknowledge support and funding from the FP7/2007-2013 under grant agreement no. 264098-MAMA. VBZ acknowledges EU support during measurements at the synchrotron facility Helmholtz–Zentrum Berlin für Materialien und Energie HZB.

References

[1] Ruddlesden S N and Popper P 1958 *Acta Crystallogr.* **11** 54
[2] Maeno Y, Hashimoto H, Yoshida K, Nishizaki S, Fujita T, Bendorz J G and Lichtenberg F 1994 *Nature* **372** 532
[3] Kallin C and Berlinsky A J 2009 *J. Phys.: Condens. Matter* **21** 164210
[4] Perry R S *et al* 2001 *Phys. Rev. Lett.* **86** 2661
[5] Grigera S A *et al* 2004 *Science* **306** 1154
[6] Grigera S A, Perry R S, Schofield A J, Chiao M, Julian S R, Lonzarich G G, Ikeda S I, Maeno Y, Millis A J and Mackenzie A P 2001 *Science* **294** 329
[7] Haverkort M W, Elfimov I S, Tjeng L H, Sawatzky G A and Damascelli A 2008 *Phys. Rev. Lett.* **101** 026406
[8] Pavarini E and Mazin I I 2006 *Phys. Rev.* B **74** 035115
[9] Oguchi T 2009 *J. Phys. Soc. Japan* **78** 044702
[10] Iwasawa H, Yoshida Y, Hase I, Koikegami S, Hayashi H, Jiang J, Shimada K, Namatame H, Taniguchi M and Aiura Y 2010 *Phys. Rev. Lett.* **105** 226406
[11] Rozbicki E J, Annett J F, Souquet J-R and Mackenzie A P 2011 *J. Phys.: Condens. Matter* **23** 094201
[12] Shen K M *et al* 2001 *Phys. Rev.* B **64** 180502
[13] Damascelli A *et al* 2000 *Phys. Rev. Lett.* **85** 5194
[14] Iwasawa H *et al* 2005 *Phys. Rev.* B **72** 104514
[15] Shen K M, Kikugawa N, Bergemann C, Balicas L, Baumberger F, Meevasana W, Ingle N J C, Maeno Y, Shen Z-X and Mackenzie A P 2007 *Phys. Rev. Lett.* **99** 187001
[16] Sekiyama A *et al* 2004 *Phys. Rev.* B **70** 060506
[17] Oguchi T 1995 *Phys. Rev.* B **51** 1385
[18] Singh D J 1995 *Phys. Rev.* B **52** 1358
[19] Hase I and Nishihara Y 1996 *J. Phys. Soc. Japan* **65** 3957
[20] Hiraoka N, Buslaps T, Honkimäki V, Nomura T, Itou M, Sakurai Y, Mao Z Q and Maeno Y 2006 *Phys. Rev.* B **74** 100501
[21] Bergemann C, Mackenzie A P, Julian S R, Forsythe D and Ohmichi E 2003 *Adv. Phys.* **52** 639
[22] Matzdorf R, Fang Z, Ismail Zhang J, Kimura T, Tokura Y, Terakura K and Plummer E W 2000 *Science* **289** 746
[23] Ingle N J C *et al* 2005 *Phys. Rev.* B **72** 205114
[24] Iwasawa H, Aiura Y, Saitoh T, Yoshida Y, Hase I, Ikeda S and Bando H 2006 *Physica* C **445–8** 73
[25] Aiura Y, Yoshida Y, Hase I, Ikeda S I, Higashiguchi M, Cui X Y, Shimada K, Namatame H, Taniguchi M and Bando H 2004 *Phys. Rev. Lett.* **93** 117005
[26] Kidd T E, Valla T, Fedorov A V, Johnson P D, Cava R J and Haas M K 2005 *Phys. Rev. Lett.* **94** 107003
[27] Pennec Y, Ingle N J C, Elfimov I S, Varene E, Maeno Y, Damascelli A and Barh J V 2008 *Phys. Rev. Lett.* **101** 216103
[28] Shevchik N J 1977 *Phys. Rev.* B **16** 3428
[29] Theilmann F, Matzdorf R, Meister G and Goldmann A 1997 *Phys. Rev.* B **56** 3632
[30] Cerrina F, Myron J R and Lapeyre G J 1984 *Phys. Rev.* B **29** 1798
[31] Kikugawa N, Mackenzie A P and Maeno Y 2003 *J. Phys. Soc. Japan* **72** 237
[32] Gies P and Gerhardts R R 1986 *Europhys. Lett.* **1** 513
[33] Meyers B C and Feuchtwang T E 1983 *Phys. Rev.* B **27** 2030
[34] Gerhardts R R 1983 *Phys. Scr.* **28** 235
[35] Levinson H J and Plummer E W 1981 *Phys. Rev.* B **24** 628

[36] Levinson H J, Plummer E W and Feibelman P J 1979 *Phys. Rev. Lett.* **43** 952
[37] Leventi-Peetz A, Krasovskii E E and Schattke W 1995 *Phys. Rev.* B **51** 17965
[38] Krasovskii E E, Silkin V M, Nazarov V U, Echenique P M and Chulkov E V 2010 *Phys. Rev.* B **82** 125102
[39] Krasovskii E E and Schattke W 1999 *Phys. Rev.* B **60** R16251
[40] Schaich W L and Kempa K 1987 *Phys. Scr.* **35** 204
[41] Feibelman P J 1982 *Prog. Surf. Sci.* **12** 287
[42] Feuerbacher B and Willis R F 1976 *J. Phys. C: Solid State* **9** 169
[43] Das P and Kar N 1995 *Phys. Status Solidi* b **187** 551
[44] Mukhopadhyay G and Lundqvist S 1978 *Phys. Scr.* **17** 69
[45] Feibelman P J 1975 *Phys. Rev. Lett.* **34** 1092
[46] Feibelman P J 1975 *Phys. Rev.* B **12** 1319
[47] Samuelsen D and Schattke W 1995 *Phys. Rev.* B **51** 2537
[48] Zabolotnyy V B *et al* 2007 *Phys. Rev.* B **76** 024502
[49] Dubs R L, Dixit S N and McKoy V 1985 *Phys. Rev.* B **32** 8389
[50] Varma C M 2006 *Phys. Rev.* B **73** 233102
[51] Kaminski A *et al* 2002 *Nature* **416** 610
[52] Borisenko S V, Kordyuk A A, Koitzsch A, Knupfer M, Fink J, Berger H and Lin C T 2004 *Nature* **431**
[53] Evtushinsky D V *et al* 2006 *Phys. Rev.* B **74** 172509
[54] Petersen L and Hedegrd P 2000 *Surf. Sci.* **459** 49
[55] Bihlmayer G, Koroteev Y, Echenique P, Chulkov E and Blgel S 2006 *Surf. Sci.* **600** 3888
[56] Nicolay G, Reinert F, Hüfner S and Blaha P 2001 *Phys. Rev.* B **65** 033407
[57] LaShell S, McDougall B A and Jensen E 1996 *Phys. Rev. Lett.* **77** 3419
[58] Rotenberg E, Chung J W and Kevan S D 1999 *Phys. Rev. Lett.* **82** 4066
[59] Earnshaw A, Figgis B N, Lewis J and Peacock R D 1961 *J. Chem. Soc.* 3132
[60] Rozbicki E J, Annett J F, Souquet J-R and Mackenzie A P 2011 *J. Phys.: Condens. Matter* **23** 094201
[61] Varykhalov A, Sánchez-Barriga J, Shikin A M, Gudat W, Eberhardt W and Rader O 2008 *Phys. Rev. Lett.* **101** 256601
[62] Putzke C *et al* 2012 *Phys. Rev. Lett.* **108** 047002
[63] Kordyuk A A, Zabolotnyy V B, Evtushinsky D V, Kim T K, Morozov I V, Kulić M L, Follath R, Behr G, Büchner B and Borisenko S V 2011 *Phys. Rev.* B **83** 134513
[64] Gray A X *et al* 2011 *Nature Mater.* **10** 759
[65] Papp C, Plucinski L, Minar J, Braun J, Ebert H, Schneider C M and Fadley C S 2011 *Phys. Rev.* B **84** 045433
[66] Kamakura N, Takata Y, Tokushima T, Harada Y, Chainani A, Kobayashi K and Shin S 2006 *Phys. Rev.* B **74** 045127